Inorganic Chemistry

ARTICLE

pubs.acs.org/IC

Non-Innocent Ligand Behavior of a Bimetallic Ni Schiff-Base Complex Containing a Bridging Catecholate

Tim J. Dunn,[†] Caterina F. Ramogida,[†] Curtis Simmonds,[†] Alisa Paterson,[†] Edwin W. Y. Wong,[†] Linus Chiang,[†] Yuichi Shimazaki,[‡] and Tim Storr*[,†]

[†]Department of Chemistry, Simon Fraser University, Burnaby, British Columbia V5A-1S6, Canada

[‡]College of Science, Ibaraki University, Bunkyo, Mito 310-8512, Japan

Supporting Information

ABSTRACT: The geometric and electronic structure of a bimetallic Ni Schiff-base complex and its one-electron oxidized form have been investigated in the solid state and in solution. The two salen units in the neutral complex **1** are linked via a bridging catecholate function. The one-electron oxidized form $[\mathbf{1}]^+$ was determined to exist as a ligand radical species in solution, with the electron hole potentially localized on the redox-active dioxolene, the phenolate ligands, or delocalized over the entire ligand system. Electrochemical experiments and UV−vis−NIR spectroscopy, in combination with density functional theory (DFT) calculations, provide insight into the locus of oxidation and the degree of delocalization in this system. The one-electron hole for $[\mathbf{1}]^+$ was determined experimentally to be localized on the dioxolene bridge with a small amount of spin density on the outer phenolate moieties predicted by the calculations. The resonance Raman spectrum of $[\mathbf{1}]^+$ (λ_{ex} = 413 nm) in CH_2Cl_2 solution clearly exhibited a new band at 1315 cm^{-1} in comparison to **1**, which is predicted to be a combination of dioxolene ring and C−O bond stretching modes, consistent with oxidation of the bridging moiety in $[\mathbf{1}]^+$. Analysis of the NIR bands for $[\mathbf{1}]^+$, in association with time-dependent DFT calculations, suggests that the low energy bands are ligand to ligand charge transfer transitions from the terminal phenolates to the central dioxolene unit. In combination, this data is consistent with a description of the overall electronic structure of $[\mathbf{1}]^+$ as a bridge-localized semiquinone ligand radical species. This is in contrast to the mixed-valence ground state description for many one-electron oxidized Ni salen monomer systems, and analysis in terms of intervalence charge transfer (IVCT) theory.

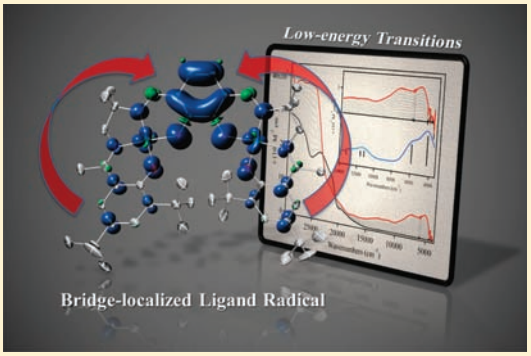

1. INTRODUCTION

The redox chemistry of transition metal complexes with pro-radical ligands, and the correlation of reactivity with electronic structure, continues to be an area of considerable research interest.[1] This work is inspired by metalloenzyme systems, where the interaction of redox-active transition metal ions and pro-radical ligands is well established.[2,3] Galactose oxidase is a classic example,[3] catalyzing the aerobic oxidation of primary alcohols to aldehydes via two one-electron cofactors: a copper atom and a cysteine-modified tyrosine residue. Many reports have documented the non-innocent[4−6] character of ligands such as the dioxolenes,[6] dithiolenes,[7] phenolates,[8,9] *o*-phenylenediamines,[10] amidophenolates,[11,12] and salens.[13−19] This research has led to an improved understanding of the interaction between transition metals and non-innocent ligands, and to the development of small molecule systems that incorporate redox-active ligands into catalyst design.[12,20]

Tetradentate salen ligands (salen is a common abbreviation for N_2O_2 bis-Schiff-base bis-phenolate ligands) have received considerable attention as ligand systems because of their relative ease of synthesis, ability to form stable complexes with many metals in a variety of oxidation states, and versatility as catalysts for organic transformations.[21] More recently, the non-innocent character of salen ligands has been documented.[13−19] Depending on the relative energies of the redox-active orbitals, metal complexes with non-innocent ligands exist in two limiting descriptions, either a metal−ligand radical ($M^{n+}(L^{\bullet})$) or a high valent metal ($M^{(n+1)+}(L^{-})$) complex. As an example, one-electron oxidation of **NiSal^{tBu}** (Chart 1) affords a ligand radical complex in the solid state and in solution.[17,19] Sterically demanding *ortho* and *para* substituents on the phenolates are critical for the stabilization of the oxidized metal salen complexes, which are prone to rapid polymerization.[22] Interestingly, in the presence of coordinating solvent or counterions, a shift in the locus of oxidation is observed to form a Ni(III) complex.[13,17,19,23,24] These studies highlight how modulation of the ligand field via axial ligand binding can shift the locus of oxidation within the complex.

Received: April 17, 2011
Published: June 15, 2011

Chart 1. Structures of NiSal^{tBu} and the Bimetallic Analogue 1

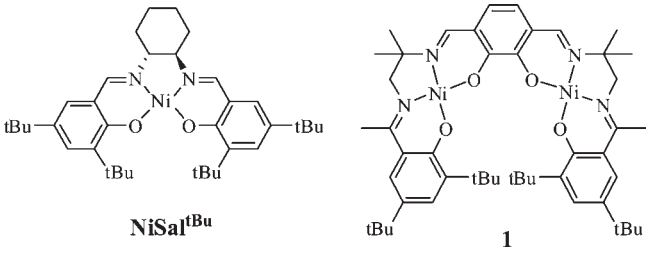

NiSal^{tBu} 1

Multimetallic Schiff-base compounds exhibit considerable potential as catalysts,[25] sensors for small molecules and ions,[26,27] magnetic materials,[28−30] and as self-assembled functional materials.[31,32] While broadly investigated as catalysts, the ligand radical chemistry of multimetallic salen complexes has received little attention.[15,23,29,30] In this work we have studied the oxidative chemistry of a bimetallic Ni Schiff-base complex **1** employing a bridging dioxolene (Chart 1). The dioxolene linker is derived from 3,6-diformyldihydroxybenzene[33] which has been used extensively in the formation of Schiff-base macrocyclic compounds.[32,34] The oxidative chemistry of **1** is of interest as the ligand is effectively a combination of redox-active dioxolene and phenolate ligands. Using a combination of experiments and calculations, we show that oxidation of **1** affords a semiquinone ligand radical species, in which the oxidation is localized on the electron-rich bridging unit.

2. EXPERIMENTAL SECTION

2.1. Materials and Methods. All chemicals used were of the highest grade available and were further purified whenever necessary.[35] 3,6-Diformyldihydroxybenzene[33] (**2**), 2-acetyl-4,6-di-*tert*-butylphenol,[36] and $[N(C_6H_3Br_2)_3]SbF_6$[37] were prepared according to literature procedures. Electronic spectra were obtained on a Cary 5000 spectrophotometer with a custom-designed immersible fiber-optic quartz probe with variable path length (1 and 10 mm; Hellma, Inc.). Constant temperatures were maintained by a dry ice/acetone bath. Solvent contraction was accounted for in all variable-temperature studies. Cyclic voltammetry (CV) was performed on a PAR-263A potentiometer, equipped with a Ag wire reference electrode, a platinum disk working electrode, and a Pt counter electrode with 0.1 M NBu_4ClO_4 solutions in CH_2Cl_2. Ferrocene was used as an internal standard. ^1H and $^{13}C\{^1H\}$ NMR spectra were recorded on Bruker AV-400 or AV-600 instruments. Mass spectra (positive ion) were obtained on an Agilent 6210 TOF ESI-MS instrument. Elemental analyses (C, H, N) were performed by Mr. Farzad Haftbaradaran at Simon Fraser University on a Carlo Erba EA1110 CHN elemental analyzer. Resonance Raman spectra were obtained on a SpectraPro-300i spectrometer (Acton Research) with a 2400-groove grating, a Beamlok 2060 Kr ion laser (Spectra-Physics), a holographic supernoch filter (Kaiser Optical Systems), and a LN-1100PB CCD detector (Princeton Instruments) cooled with liquid N_2. Spectra were collected on solvated samples in spinning cells (2 cm diameter, 1500 rpm) at 213 K at an excitation wavelength λ_{ex} = 413.1 nm (15 mW), 90° scattering geometry, and 5 min data accumulation. Peak frequencies were calibrated relative to indene and CCl_4 standards (accurate to ±1 cm^{-1}). During each Raman experiment, UV−vis spectra were simultaneously collected on a PMA-11 CCD spectrophotometer (Hamamatsu) with a Photal MC-2530 (D2/W2) light source (Otsuka Electronic Co.). All electron paramagnetic resonance (EPR) spectra were collected using a Bruker EMXplus spectrometer operating with a premiumX X-band (~9.5 GHz) microwave bridge. Low temperature measurements of frozen solutions used a Bruker helium temperature-control system and a continuous flow cryostat. Samples for X-band measurements were placed in 4 mm outer-diameter sample tubes with sample volumes of ~300 μL. EPR spectra were simulated with EasySpin 3.1.7 software.[38]

2.2. Synthesis. *2.2.1. (2-(1-(2-Amino-2-methylpropylimino)ethyl)-4,6-di-tert-butylphenol) (**3**).* In a reaction vessel equipped with 3 Å molecular sieves under a nitrogen atmosphere, 1,2-diamino-2-methylpropane (0.63 g, 7.1 mmol, 1.5 equiv) in anhydrous MeOH (7 mL) was added to 2-acetyl-4,6-di-*tert*-butylphenol (1.18 g, 4.77 mmol). The reaction mixture was brought to reflux and left to stir for 7 h, after which it was cooled to ambient temperature, filtered, and concentrated in vacuo. The resulting orange oil was purified by flash chromatography using EtOAc/MeOH (1:0 to 4:1) to afford **3** (1.42 g, 94%) as a yellow solid. ^1H NMR (600 MHz, $CDCl_3$) δ = 7.40 (d, J = 2.3, 1H, Ar-*H*), 7.37 (d, J = 2.3, 1H, Ar-*H*), 3.42 (s, 2H, CH_2), 2.35 (s, 3H, CH_3), 1.43 (s, 9H, *t*-Bu), 1.30 (s, 9H, *t*-Bu), 1.24 (s, 6H, 2 × CH_3); $^{13}C\{^1H\}$ NMR (151 MHz, $CDCl_3$) δ = 172.70, 160.52, 138.06, 137.58, 126.99, 122.11, 118.35, 62.63, 50.43, 35.23, 34.26, 31.59, 29.48, 29.36, 28.85, 15.15; ESI m/z (%): 319.27 (100) $[\mathbf{3} + H]^+$; anal. calcd. (found) for $C_{20}H_{34}N_2O_1 \cdot H_2O$: C 71.38 (71.31), H 10.78 (10.33), N 8.32 (8.25).

2.2.2. Synthesis of H_4L. 3,6-Diformyldihydroxybenzene (**2**) (0.236 g, 1.42 mmol) and monoimine **3** (0.950 g, 2.98 mmol, 2.1 equiv) were dissolved with heating in MeOH (10 mL). The solution was left to stir for 16 h while cooling to ambient temperature. The mixture was cooled in a freezer, and the resulting precipitate was filtered and dried in vacuo to produce $\mathbf{H_4L}$ as a yellow powder (0.810 g, 74%). ^1H NMR (400 MHz, $CDCl_3$) δ = 8.35 (s, 2H, NC*H*), 7.35 (d, J = 2.4, 2H, Ar-*H*), 7.33 (d, J = 2.4, 2H, Ar-*H*), 6.74 (s, 2H, Ar-*H*), 3.68 (s, 4H, CH_2), 2.31 (s, 6H, CH_3), 1.48 (s, 12H, 2 × CH_3), 1.39 (s, 18H, *t-Bu*), 1.26 (s, 18H, *t-Bu*); $^{13}C\{^1H\}$ NMR (101 MHz, CD_2Cl_2) δ = 173.25, 161.90, 160.23, 151.11, 138.08, 137.13, 126.83, 122.32, 120.14, 119.54, 118.34, 60.58, 35.01, 34.11, 31.27, 29.17, 25.05, 15.06; ESI m/z (%): 767.55 (100) $[\mathbf{H_4L} + H]^+$; anal. calcd. (found) for $C_{48}H_{70}N_4O_4$: C 75.16 (74.77), H 9.20 (8.80), N 7.30 (7.29).

*2.2.3. Synthesis of Ni_2L (**1**).* To a solution of $\mathbf{H_4L}$ (0.154 g, 0.20 mmol) in CH_2Cl_2/MeOH (1:3, 6 mL) was added a solution of Ni(OAc)$_2 \cdot 4H_2O$ (0.100 g, 0.40 mmol, 2 equiv) in MeOH (2 mL), followed by triethylamine (112 μL, 0.803 mmol, 4 equiv). The mixture was stirred at ambient temperature for 3 h and then concentrated down to 2 mL and cooled in the freezer. The resulting precipitate was filtered, washed with cold MeOH (1 mL) and H_2O (1 mL), and then dried in vacuo to yield a brown solid. The solid was dissolved in CH_2Cl_2/MeOH (5:2) and slow evaporation afforded dark red crystals of **1** (0.137 g, 94%). ^1H NMR (400 MHz, $CDCl_3$) δ = 7.21 (d, J = 2.2, 2H, Ar-*H*), 7.14 (s, 2H, NC*H*), 7.12 (d, J = 2.2, 2H, Ar-*H*), 6.11 (s, 2H, Ar-*H*), 3.33 (s, 4H, CH_2), 2.30 (s, 6H, CH_3), 1.35 (s, 18H, *t*-Bu), 1.27 (s, 12H, 2 × CH_3), 1.25 (s, 18H, *t*-Bu); $^{13}C\{^1H\}$ NMR (101 MHz, CD_2Cl_2) δ = 168.57, 162.65, 159.60, 158.37, 141.28, 134.73, 126.80, 122.54, 122.11, 119.09, 115.44, 67.30, 63.68, 35.48, 33.94, 31.17, 29.87, 25.99, 18.53; ESI m/z (%): 901.37 (100) $[\mathbf{1} + Na]^+$; anal. calcd. (found) for $C_{48}H_{66}O_4N_4Ni_2$: C 65.48 (65.31), H 7.56 (7.58), N 6.36 (6.34).

2.2.4. Synthesis of $[Ni_2L]^+$ ($[\mathbf{1}]^+$). Method 1. Under an inert atmosphere, $NOSbF_6$ (0.0046 g, 0.017 mmol) was slowly added to a solution of **1** (0.015 g, 0.017 mmol) in CH_2Cl_2. The resulting mixture was stirred at ambient temperature for 1 h; the solvent was then removed under reduced pressure to produce $[\mathbf{1}]^+ SbF_6^-$ as a dark green solid.

2.2.5. Synthesis of $[Ni_2L]^+$ ($[\mathbf{1}]^+$). Method 2. Under an inert atmosphere, a solution of $[N(C_6H_3Br_2)_3^{\bullet}]^+ SbF_6^-$ (1 equiv) in CH_2Cl_2 was added in aliquots to a solution of **1** in CH_2Cl_2 at low temperature (198 K), forming $[\mathbf{1}]^+ SbF_6^-$. The oxidation process was monitored by UV−vis−NIR spectroscopy. Repeating the experiment at 298 K afforded similar results, however the near-infrared (NIR) bands were not as well resolved (Supporting Information, Figure S1).

dx.doi.org/10.1021/ic200785g |*Inorg. Chem.* 2011, 50, 6746–6755

2.3. X-ray Structure Determination. Single crystal X-ray crystallographic analysis of **1** was performed on a Bruker X8 APEX II diffractometer with graphite monochromated Mo−Kα radiation. A red needle crystal of $C_{48}H_{66}N_4O_4Ni_2 \cdot 1.5C_6H_{14}$, isolated from the slow evaporation of a 1:1 CH_2Cl_2:hexanes solution and having approximate dimensions of 0.12 × 0.24 × 0.55 mm, was mounted on a glass fiber. The data were collected at a temperature of −100.0 ± 0.1 °C to a maximum 2θ value of 50.3°. Data were collected in a series of φ and ω scans in 0.50° oscillations with 30.0 s exposures. The crystal-to-detector distance was 36.00 mm. The structure was solved by direct methods.[39] The material crystallizes with disordered solvent in the lattice. Unfortunately the solvent was disordered to such an extent that it could not be properly modeled. The PLATON/SQUEEZE[40] program was used to generate a "solvent-free" data set, and the results suggest one and one-half molecules of hexanes were present in the asymmetric unit (3 per unit cell). The formula and any values calculated from it subsequently were adjusted to reflect the presence of 1.5 molecules of C_6H_{14} per asymmetric unit. Additionally, two *t*-butyl groups were disordered and the methyl carbons were modeled in two different orientations. All non-hydrogen atoms except the minor disordered *t*-butyl carbons were refined anisotropically.

Single crystal X-ray crystallographic analysis of $[\mathbf{1}\cdot Ag]^+SbF_6^-$ was performed at room temperature on a Bruker SMART diffractometer equipped with an APEX II CCD area detector fixed at a distance of 60 mm from the crystal and a Mo−Kα fine focus sealed tube operated at 1.5 kW (50 kV, 30 mA) with a graphite monochromator. A red-orange plate with the approximate dimensions of 0.3 × 0.12 × 0.03 mm was isolated from layering hexanes over a CH_2Cl_2 solution of $[\mathbf{1}\cdot Ag]^+SbF_6^-$ and mounted on a glass fiber using epoxy resin. All frames were collected using a scan width of 0.5° in φ and ω with 60 s exposures. The structure was solved using direct methods (SIR92)[39] and refined by least-squares procedures using CRYSTALS (v14.23a).[41] The crystal diffracted poorly and consequently, there was only enough data to refine the heavy atoms (Ni, Ag, Sb) anisotropically. All other atoms were refined isotropically. Hydrogen atoms were placed in idealized geometric positions and linked to their respective carbon atoms using a riding model during refinement. The isotropic temperature factor of each hydrogen atom was initially set to 1.2 times that of the carbon atom it is bonded to and then the temperature factors of groups of similar hydrogen atoms were linked during refinement. All crystal structure plots were produced using ORTEP-3 and rendered with POV-Ray (v. 3.6.2). A summary of the crystal data and experimental parameters for structure determinations are given in Table 1.

2.4. Calculations. Geometry optimizations and single point calculations were performed using the Gaussian 09 program (Revision A.02),[42] the B3LYP functional,[43] and the TZVP basis set of Ahlrichs[44] on all atoms. Frequency calculations at the same level of theory confirmed that the optimized structures were located at a minimum on the potential energy surface. The intensities of the 30 lowest-energy electronic transitions were calculated by TD-DFT[45,46] at the B3LYP/TZVP level with a polarized continuum model (PCM) for CH_2Cl_2 (dielectric $\varepsilon = 8.94$).[47] AOMix[48] was used for determining atomic orbital compositions employing Mulliken Population Analysis.

3. RESULTS AND ANALYSIS

3.1. Synthesis and Characterization of Ni Complex 1. *3.1.1. Synthesis and Characterization of* ***1***. The synthesis of the symmetrical Schiff-base binucleating ligand proceeds in a facile manner from 2 equiv of an asymmetric monoimine precursor **3** and 3,6-diformyldihydroxybenzene **2** (Scheme 1). The asymmetric monoimine precursor **3** was synthesized using the route developed by Bottcher et al.,[49] where an asymmetric diamine is reacted with a ketone to produce **3**. The *t*-butyl groups were incorporated into the design to prevent radical coupling, as oxidized metal salen complexes are prone to rapid polymerization.[22] The ligand $\mathbf{H_4L}$ was reacted with $Ni(OAc)_2\cdot 4H_2O$ to form complex **1**. Characterization of **1** is consistent with the formation of a neutral bimetallic d^8 square-planar bis-Ni complex.

3.1.2. Solid State Characterization of ***1***. Single crystals suitable for X-ray analysis were isolated by slow evaporation of a concentrated CH_2Cl_2/hexanes solution of **1**. The molecular structure of **1** is shown in Figure 1, and selected crystallographic data for the complex is presented in Table 1. The solid state structure of **1** exhibits a slightly distorted square planar geometry at each Ni center, with the expected N_2O_2 coordination sphere; the dihedral angle between the N−Ni−O planes is 11.5° (Ni(1)) and 12.6° (Ni(2)). Overall, the molecule is not flat, with a significant twist in the structure because of a steric interaction of the two ortho *t*-butyl groups (Supporting Information, Figure S2). The angle between the two outer phenolate ring planes is 58.9°. In addition, there is a slight difference in the Ni(1)−O(1)/Ni(1)−O(4) and Ni(2)−O(2)/Ni(2)−O(3) bond lengths in the structure (Table 2). The $Ni-O_{catecholate}$ bond lengths are longer (1.87 Å) in comparison to the $Ni-O_{phenolate}$ bond lengths (1.82 Å). The difference in the Ni−N bond lengths in the structure is much less (Table 2), and overall the structure is essentially C_2-symmetric. This matches with the symmetry evident in ^{1}H NMR spectrum for both $\mathbf{H_4L}$ and **1**. The distance between the two Ni centers in the bimetallic complex is 6.4 Å.

3.2. Theoretical Characterization of 1. Density functional theory (DFT) calculations on **1** well reproduce the coordination sphere bond lengths and overall structure of the molecule (Table 2). The predicted Ni−N bond lengths are within ±0.04 Å of the experimental values. While the predicted $Ni-O_{catecholate}$ bond lengths (Ni(1)−O(1) and Ni(2)−O(2)) closely match the

Table 1. Selected Crystallographic Data for 1 and $[\mathbf{1}\cdot Ag]^+SbF_6^-$

formula	$C_{48}H_{66}N_4O_4Ni_2$	$C_{48}H_{66}N_4O_4Ni_2AgSbF_6$
formula weight (g mol^{-1})	880.43	1224.10
space group	$P\bar{1}$ (#2)	$P\bar{1}$ (#2)
a (Å)	11.9216(5)	11.4055(17)
b (Å)	13.4517(6)	13.230(2)
c (Å)	18.7042(7)	17.620(3)
α (deg)	110.218(5)	105.773(2)
β (deg)	98.147(5)	90.269(2)
γ (deg)	100.074(5)	91.001(2)
V (Å^3)	2704.14(19)	2558.1(7)
Z	2	2
T (°C)	−100	23
ρ_{calcd} (g cm^{-3})	1.240	1.589
λ (Å) (graphite monochromatized)	0.71073 (Mo Kα)	0.71073 (Mo Kα)
μ (MoKα) (cm^{-1})	7.44	1.69
R indices[a] with $I > 2\sigma(I)$ (data)	6002	2965
wR_2	0.133	0.103
R_1	0.089	0.083
goodness-of-fits on F^2	0.98	1.82[a]

[a] Goodness-of-fit on *F*.

dx.doi.org/10.1021/ic200785g |*Inorg. Chem.* 2011, 50, 6746–6755

Scheme 1. Synthesis of the Ligand H_4L and Bimetallic Ni Salen Complex 1[a]

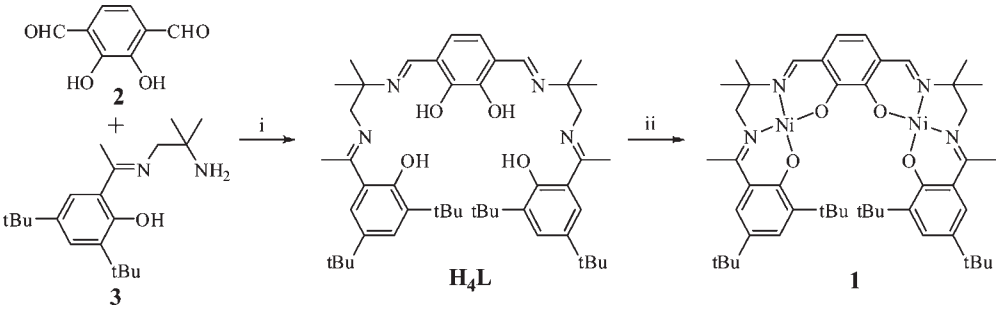

[a] (i) MeOH, 2 equiv of **3**; (ii) $Ni(OAc)_2$, MeOH.

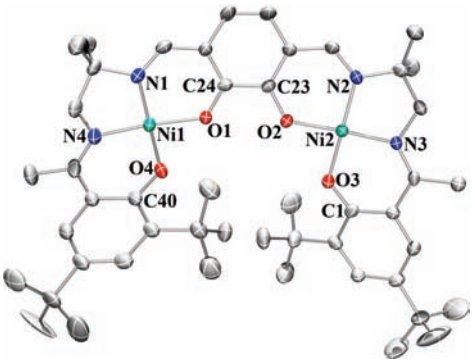

Figure 1. Molecular structure of **1**, excluding hydrogen atoms. Thermal ellipsoids are set at 50% probability. Selected interatomic distances (Å) and angles (deg): Ni(1)−O(1), 1.872(2); Ni(1)−O(4), 1.821(2); Ni(1)−N(1), 1.841(3); Ni(1)−N(4), 1.855(3); Ni(2)−O(2), 1.869(2); Ni(2)−O(3), 1.817(2); Ni(2)−N(2), 1.846(3); Ni(2)−N(3), 1.857(2); Ni(1)···Ni(2), 6.405; O(1)−Ni(1)−O(4), 85.7(1); O(1)−Ni(1)−N(1), 94.4(1); O(4)−Ni(1)−N(4), 94.2(1); N(1)−Ni(1)−N(4), 87.0(1); O(2)−Ni(2)−O(3), 85.8(1); O(2)−Ni(2)−N(2), 94.6(1); O(3)−Ni(2)−N(3), 93.8(1); N(2)−Ni(2)−N(3), 87.3(1).

Table 2. Experimental and Calculated Coordination Sphere Metrical Parameters for the Complexes (in Å)

bond	**1** (Å) experiment	**1** (Å) calculated	$[\mathbf{1}]^+$ (Å) calculated
Ni(1)−N(1)	1.841	1.877	1.864
Ni(1)−N(4)	1.855	1.877	1.881
Ni(2)−N(2)	1.846	1.877	1.881
Ni(2)−N(3)	1.857	1.877	1.864
Ni(1)−O(1)	1.872	1.876	1.886
Ni(1)−O(4)	1.821	1.851	1.827
Ni(2)−O(2)	1.869	1.876	1.886
Ni(2)−O(3)	1.817	1.851	1.828
Ni(1)−Ni(2)	6.405	6.294	6.289

experimental values, the calculated Ni−$O_{phenolate}$ bond lengths (Ni(1)−O(4) and Ni(2)−O(3)) are longer by about 0.03 Å. The predicted angle between the two outer phenolate rings (75.0°) is larger than the experimental value (58.9°), with packing effects in the solid state likely responsible for this difference.

3.3. Electrochemistry. The redox activity of H_4L and **1** were probed by cyclic voltammetry (CV). At 298 K the redox processes for H_4L were irreversible and thus the CV experiments were performed at 233 K (Figure 2). The first redox process for H_4L is quasi-reversible at 233 K and demonstrates the instability of the ligand in the oxidized form; continued scanning to more positive potentials results in decomposition and irreversibility for the redox process at 209 mV (Supporting Information, Figure S3). In comparison, **1** displays two reversible redox couples at 75 mV and 690 mV vs Fc^+/Fc. The first redox couple for **1** is a one-electron process, while the redox-couple at higher potential is a two-electron process (Figure 2). The reversibility of the first redox process is noticeably improved upon metal binding, and shifts to lower potentials demonstrating a slight increase in electron density at the site of oxidation.[50] In addition, the first redox process for **1** occurs at a much lower potential in comparison to similar Ni salen monomeric complexes such as $\mathbf{NiSal}^{\mathbf{tBu}}$ (Table 3).[19,51] The first redox process for **1** is centered on the ligand on the basis of the experimental results (vide infra),

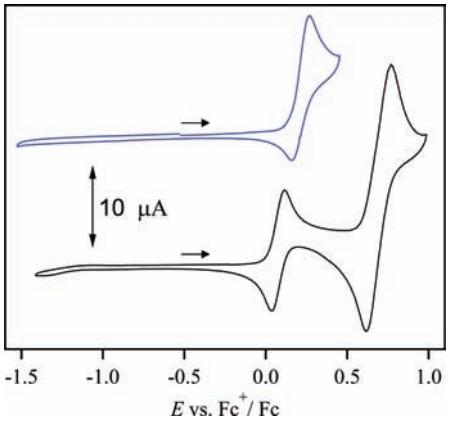

Figure 2. Cyclic voltammograms of H_4L (blue) and **1** (black). Conditions: 1 mM complex, 0.1 M NBu_4ClO_4, scan rate 100 mV/s, CH_2Cl_2, 233 K.

Table 3. Redox Potentials for H_4L, and 1 versus Fc^+/Fc[a]

compound	$E_{1/2}{}^1$/mV	$E_{1/2}{}^2$/mV	$\Delta E_{ox}(E_{1/2}{}^2 - E_{1/2}{}^1)$/mV
H_4L	210 (100)		
1	75 (68)	690 (160)	620
$\mathbf{NiSal}^{\mathbf{tBu}}$ [b]	450	950	500

[a] Peak to peak differences in brackets ($|E_{pa} - E_{pc}|$ in mV). Peak to peak difference for the Fc^+/Fc couple at 230 K is 70 mV. Conditions: 1 mM complex, 0.1 M NBu_4ClO_4, scan rate 100 mV/s, CH_2Cl_2, 233 K. [b] Ref 19.

dx.doi.org/10.1021/ic200785g |*Inorg. Chem.* 2011, 50, 6746–6755

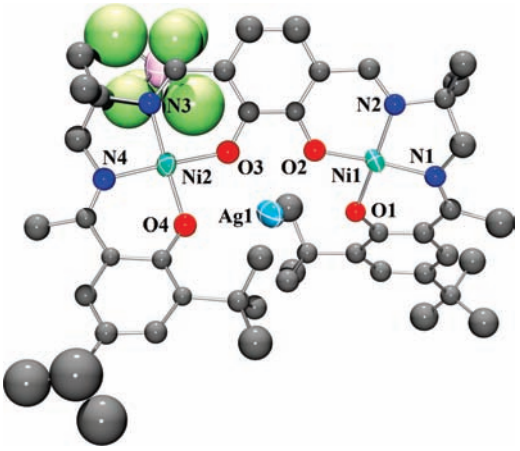

Figure 3. Molecular structure of the $[\mathbf{1}\cdot Ag]^+SbF_6^-$ adduct, excluding hydrogen atoms. The Ag, Ni, and Sb atoms were modeled anisotropically. All other atoms modeled isotropically in the structure.

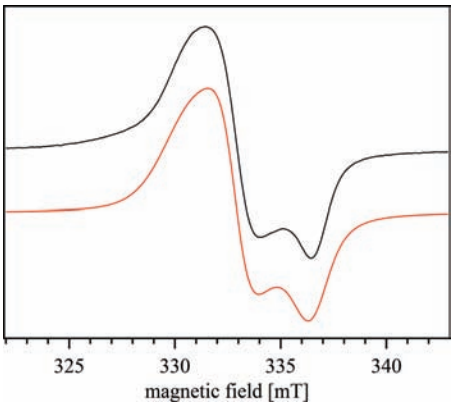

Figure 4. X-Band EPR spectra of $[\mathbf{1}^\bullet]^+$ recorded in frozen CH_2Cl_2 (3 mM) at 20 K (experimental spectra, black; simulation, red). Simulated values; g_{11} = 1.99, g_{22} = 2.01, g_{33} = 2.03, g_{av} = 2.01.

and the electrochemical data aids in the assignment of this one-electron redox process to the central catecholate to form a semiquinone radical species $[\mathbf{1}^\bullet]^+$. This assignment matches the additional data presented herein. The reversible two-electron process for **1** at higher potential is tentatively assigned to the uncoupled oxidation of both the outer phenolate moieties to form phenoxyl radicals.

3.4. Characterization of One-Electron Oxidized $[\mathbf{1}]^+$. *3.4.1. Preparation of $[\mathbf{1}]^+$.* Chemical oxidation of **1** in solution with one equiv of $AgSbF_6$ ($E_{1/2}$ = 650 mV vs Fc^+/Fc in CH_2Cl_2) did not afford the expected cation $[\mathbf{1}^\bullet]^+SbF_6^-$ in appreciable yield, even though significant driving force exists.[52] In addition, very little Ag^0 precipitate was observed in solution. Slow diffusion of hexane into a concentrated 1:1 mixture of **1** and $AgSbF_6$ in CH_2Cl_2 afforded a red crystalline material suitable for X-ray analysis. The molecular structure of $[\mathbf{1}\cdot Ag]^+SbF_6^-$ is shown in Figure 3, and selected crystallographic data for the complex is presented in Table 1. The data shows that **1** acts as a metallohost for the Ag^+ cation via the binding pocket formed by the four oxygen donors of the Schiff-base binucleating ligand. Similar complexes have been recently demonstrated to bind metal cations,[27] and in this case Ag^+ binding prevents oxidation of **1** with this oxidant. Crystals of $[\mathbf{1}\cdot Ag]^+SbF_6^-$ diffracted poorly, which prevented an accurate bond length comparison between **1** and $[\mathbf{1}\cdot Ag]^+SbF_6^-$ in the solid state, but the identity and connectivity of the compound is clear. The electrochemistry of $[\mathbf{1}\cdot Ag]^+SbF_6^-$ was complicated due to the presence of a series of irreversible redox processes, and so was not pursued further. Because of the formation of the adduct $[\mathbf{1}\cdot Ag]^+SbF_6^-$, the chemical oxidants NO^+ SbF_6^- and the aminium radical cation $[N(C_6H_3Br_2)_3^\bullet]^+$ SbF_6^- were used to oxidize **1** in solution.

3.4.2. EPR Spectroscopy. The EPR spectrum of $[\mathbf{1}]^+$ in CH_2Cl_2 at 20 K exhibits a broad anisotropic (S = 1/2) signal (g_{11} = 1.99, g_{22} = 2.01, g_{33} = 2.03, g_{av} = 2.01), demonstrating that the unpaired electron is ligand-based (Figure 4). This value is comparable to oxidized Zn phenoxyl complexes,[53] and much lower than a typical Ni(III) complex (g_{av} = 2.13−2.17).[54] The g_{av} value for $[\mathbf{1}^\bullet]^+$ is significantly lower than that for $[\mathbf{NiSal}^{\mathbf{tBu}\bullet}]^+$ (g_{iso} = 2.045),[17,19] indicating a smaller contribution of the metal to the singly occupied molecular orbital (SOMO) of $[\mathbf{1}^\bullet]^+$, and greater ligand radical character. The addition of 20 equiv of pyridine to a solution of $[\mathbf{1}^\bullet]^+$ at 233 K and subsequent cooling to 20 K resulted in decomposition of the oxidized complex and a complete loss of the EPR signal (Supporting Information, Figure S4). This result differs from that for $[\mathbf{NiSal}^{\mathbf{tBu}\bullet}]^+$, where axial binding of pyridine results in modulation of the ligand field and a shift in the locus of oxidation to form a Ni(III) complex.[16,17,19,55] While we cannot rule out that a Ni(III) complex of $[\mathbf{1}^\bullet]^+$ forms upon pyridine addition, the overall stability is much lower in this case.

3.4.3. Theoretical Calculations. DFT calculations on $[\mathbf{1}^\bullet]^+$ predict metrical changes upon oxidation from the neutral species **1**, indicative of the locus of oxidation in this system. Little change in the Ni−N bond lengths, as well as the $Ni-O_{catecholate}$ bond lengths is observed in the data (Table 2); however, a slight contraction of 0.02 Å is predicted for the outer $Ni-O_{phenolate}$ bonds (Table 2), which is similar to the contraction observed experimentally upon oxidation of $\mathbf{NiSal}^{\mathbf{tBu}}$.[19] Interestingly, analysis of the predicted bonding pattern of the central catecholate moiety suggests that upon oxidation a bridging semiquinone species is formed (Supporting Information, Figure S5). The predicted spin density (Figure 5) is delocalized in $[\mathbf{1}^\bullet]^+$, with the majority of the spin density (ca. 62%) centered on the bridging dioxolene unit. A smaller amount of spin density (ca. 18%) is predicted to be localized on each of the outer phenolate moieties, which fits the predicted contraction in the outer $Ni-O_{phenolate}$ bonds.[18,19] The total spin density on the Ni centers is approximately 10%, which is less than that predicted for $[\mathbf{NiSal}^{\mathbf{tBu}\bullet}]^+$,[19] and fits with the lower value of g_{av} for $[\mathbf{1}^\bullet]^+$ (vide supra).

*3.4.4. Absorption Spectroscopy of **1** and $[\mathbf{1}^\bullet]^+$.* The electronic spectrum of **1** is typical of a low-spin d^8 square-planar bis-Ni complex (Figure 6, Table 4). An oxidation titration using $[N(C_6H_3Br_2)_3^\bullet]^+$ SbF_6^- at low temperature exhibits isosbestic points at 23400 cm^{-1} and 20650 cm^{-1}, demonstrating clean conversion to $[\mathbf{1}^\bullet]^+$ (Figure 6). The data at 298 K is comparable, although the spectrum is not as well resolved (Supporting Information, Figure S1). The oxidation titration also coincides with the appearance of low energy bands (<15000 cm^{-1}), in particular near-infrared (NIR) bands at 7500 cm^{-1} (ε = 5900 M^{-1} cm^{-1}) and 5300 cm^{-1} (ε = 6400 M^{-1} cm^{-1}). The low energy bands for $[\mathbf{1}^\bullet]^+$ are associated with the ligand radical; however, the intensities of the observed transitions are substantially weaker than the NIR band for $[\mathbf{NiSal}^{\mathbf{tBu}\bullet}]^+$ (4700 cm^{-1}, ε = 21500 M^{-1} cm^{-1}).[19] Analysis of the shape and intensity of the NIR band for $[\mathbf{NiSal}^{\mathbf{tBu}\bullet}]^+$, in combination with DFT calculations, led to

dx.doi.org/10.1021/ic200785g |*Inorg. Chem.* 2011, 50, 6746–6755

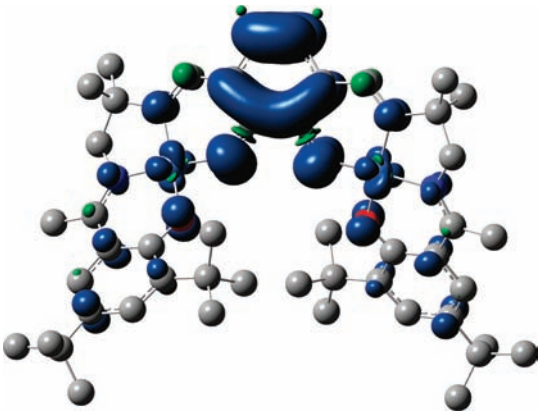

Figure 5. Calculated spin density for $[\mathbf{1}^{\bullet}]^{+}$ showing delocalization over the ligand framework with about 62% occupancy on the bridging dioxolene, 5% on each Ni center, and 18% on each terminal phenolate ligand.

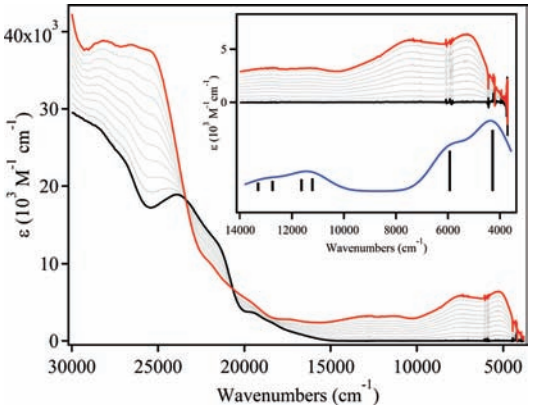

Figure 6. Electronic spectra of 0.25 mM solutions of **1** (black line), $[\mathbf{1}^{\bullet}]^{+}$ (red line) in CH_2Cl_2 at 198 K. Intermediate gray lines measured during the oxidation titration with $[N(C_6H_3Br_2)_3^{\bullet}]^{+}SbF_6^{-}$. Inset: Calculated NIR spectrum for $[\mathbf{1}^{\bullet}]^{+}$ (blue) in comparison to experimental data. Vertical lines indicate calculated low energy transitions.

classification as a Class III, fully delocalized complex based on the Robin−Day classification system.[56] TD-DFT calculations were used to gain further insight into the nature of the low energy transitions observed for $[\mathbf{1}^{\bullet}]^{+}$.

3.4.5. Theoretical Analysis of the NIR Transitions for $[\mathbf{1}^{\bullet}]^{+}$. Time-dependent density functional theory (TD-DFT) calculations[45,57] correctly predict the absence of low energy electronic transitions for **1**. The calculations do however predict a series of low energy transitions for $[\mathbf{1}^{\bullet}]^{+}$ (Figure 6 inset, Table 5), and the calculated transitions are a good match in terms of energy and intensity in comparison to the experimental data. Further analysis of the orbitals involved in the two lowest energy transitions predicts that both bands are ligand to ligand charge transfer transitions (LLCT). The higher energy band (6000 cm^{-1}) is predominantly a β-HOMO-1 → β-LUMO transition (Figure 7), with a shift in electron density from the terminal phenolates to the bridging unit. The slightly more intense band at lower energy (4300 cm^{-1}) is predicted to be a β-HOMO → β-LUMO transition (Figure 7), with a more pronounced shift in electron density from the terminal phenolates to the bridging unit. Theoretical

Table 4. Spectroscopic Properties of 1 and $[\mathbf{1}^{\bullet}]^{+}$ in CH_2Cl_2 Solution at 198 K

complex	ε_{max}, cm^{-1} ($\varepsilon \times 10^3$, M^{-1} cm^{-1})
1	28400 (27.5), 27000 (23.7), 23900 sh (18.9), 24000 (8.5), 21400 sh (12.2), 19465 (3.6), 18300 (2.3)
$[\mathbf{1}^{\bullet}]^{+}$	28100 (38.9), 26500 (38.3), 25200 sh (8.6), 25400 sh (37.3), 21900 sh (10), 19700 (5.2), 17500 (2.8), 12700 sh, (3.3), 11200 (3.2), 7500 (5.9), 5300 (6.4)

analysis suggests that the NIR bands for $[\mathbf{1}^{\bullet}]^{+}$ are best described as charge transfer transitions from the terminal phenolates to the central dioxolene moiety, consistent with a description of the overall electronic structure of $[\mathbf{1}^{\bullet}]^{+}$ as bridge-localized.[58]

*3.4.6. Resonance Raman Spectroscopy (rR) of **1** and $[\mathbf{1}^{\bullet}]^{+}$.* Resonance Raman spectroscopy (rR) is an important tool for the characterization of phenoxyl radical species.[8] Excitation in resonance with the phenoxyl $\pi \rightarrow \pi^*$ transition (ca. 400 nm) leads to the appearance of characteristic bands at ~1500 cm^{-1} (ν_{7a}, C−O stretching) and ~1600 cm^{-1} (ν_{8a}, $C_{ortho}-C_{meta}$ stretching).[53,59] In addition, rR experiments have proven very useful for the characterization of ligand oxidation states in dioxolene complexes.[60,61] The C−O stretching frequency is diagnostic of the quinone (1630−1640 cm^{-1}), semiquinone (1400−1500 cm^{-1}), or catecholate (1250−1275 cm^{-1}) oxidation level.[60] The rR spectra of **1** and $[\mathbf{1}^{\bullet}]^{+}$ in CH_2Cl_2 solution excited at 413.1 nm are shown in Figure 8. A series of weak bands are present for **1**, and the major difference upon oxidation to $[\mathbf{1}^{\bullet}]^{+}$ is the appearance of a strong band at 1315 cm^{-1}. Analysis of the rR spectrum for $[\mathbf{1}^{\bullet}]^{+}$ in the region between 1500 and 1600 cm^{-1} shows little change in comparison to **1**, and does not fit the pattern expected for phenoxyl radical formation.[17] Interestingly, the band at 1315 cm^{-1} is intermediate between that expected for a catecholate and a semiquinone. A DFT frequency calculation on the optimized structure of $[\mathbf{1}^{\bullet}]^{+}$ predicts the presence of a vibration at 1352 cm^{-1} (Supporting Information, Figure S6). This predicted vibration is assigned to ring stretching modes of the bridging moiety with mixing of C−O bond stretches (Supporting Information, Figure S7). A terminal phenolate C−O stretch is a significant component of the predicted band at 1352 cm^{-1}. The rR results, in combination with the DFT frequency analysis, support an oxidized bridging unit for $[\mathbf{1}^{\bullet}]^{+}$, with partial delocalization over the terminal phenolate moieties.

4. DISCUSSION

The synthesis of $\mathbf{H_4L}$ employed a central dialdehyde unit **2** that has been used extensively in Schiff-base macrocyclic chemistry,[32,34] and is potentially redox-active. Reaction of **2** with 2 equiv of a half-salen unit **3** developed by Bottcher et al. (Scheme 1),[49] affords $\mathbf{H_4L}$ from which the bimetallic Ni complex was synthesized in high yield. The solid state structure and further characterization data are consistent with a neutral bimetallic d^8 square-planar bis-Ni complex. The $Ni-O_{catecholate}$ bond lengths are about 0.05 Å longer than the outer $Ni-O_{phenolate}$ bond lengths, consistent with the DFT calculations (Table 2). This trend is opposite to the Ni−O bonding pattern observed by Glaser and co-workers in Ni triplesalen complexes employing a

dx.doi.org/10.1021/ic200785g |*Inorg. Chem.* 2011, 50, 6746–6755

Table 5. Predicted TD-DFT Transitions (Energies and Intensities) and Assignment for $[1^{\bullet}]^{+}$

		energy (cm^{-1})			
complex	transition (MO number)[a]	calcd	expt	oscillator strength	assignment[b]
$[1^{\bullet}]^{+}$	β-HOMO (234) → β-LUMO (235)	4300	5300	0.12	LLCT
	β-HOMO-1 (233) → β-LUMO (235)	6000	7450	0.073	LLCT
	β-HOMO-2 (232) → β-LUMO (235)	11400	11200	0.024	LLCT
	β-HOMO-4 (230) → β-LUMO (235)	12920	12900	0.012	LLCT

[a] TD-DFT (30 states); uB3LYP/TZVP (all atoms). [b] Assignment by AOMix decomposition of relevant MOs into constituent components.[48]

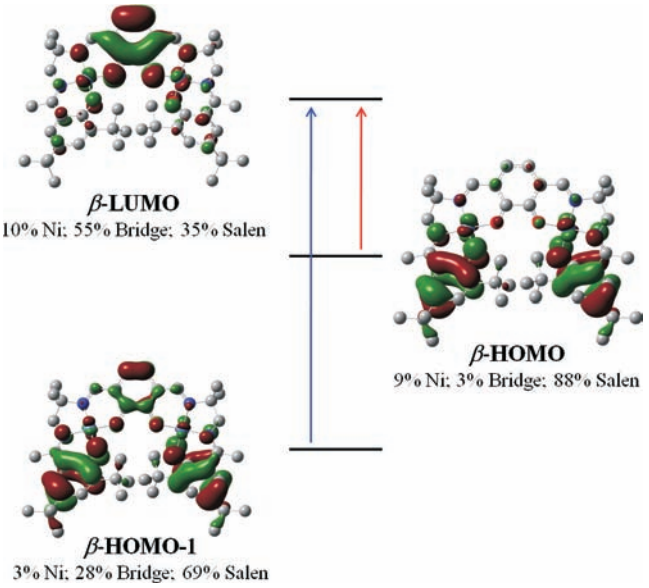

Figure 7. Kohn−Sham molecular orbitals of $[1^{\bullet}]^{+}$ associated with the calculated NIR transitions at 6000 cm^{-1} (blue arrow: β-HOMO-1 → β-LUMO), and 4300 cm^{-1} (red arrow: β-HOMO → β-LUMO). AOMix[48] MO breakdown in brackets, see Experimental Section for details.

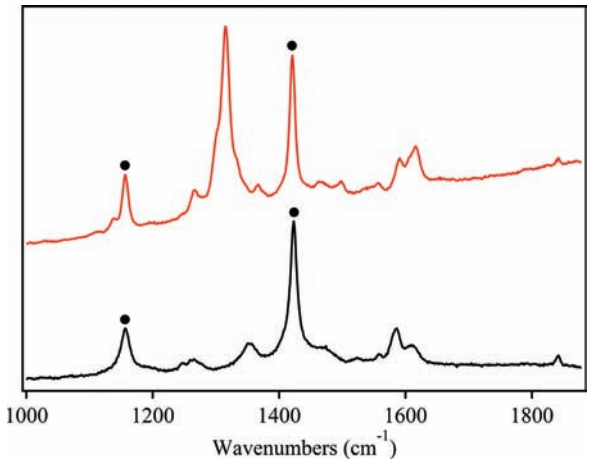

Figure 8. Resonance Raman (rR) spectra of **1** (black) and $[1^{\bullet}]^{+}$ (red) in CH_2Cl_2 at 213 K (λ_{ex} = 413 nm). Solvent = (•).

central phloroglucinol unit.[30] The twisted structure of **1**, as observed in the solid state structure, is due to the bulky *t*-butyl groups (Supporting Information, Figure S2).

CV experiments were initially employed to probe the redox properties of $\mathbf{H_4L}$ and the bimetallic Ni complex **1**. While $\mathbf{H_4L}$ could be oxidized, the redox properties were not reversible at 233 K (Figure 3, Supporting Information, Figure S3). In contrast, two reversible redox processes were observed for **1** at positive potentials. The redox processes were of particular interest as the complex is effectively a combination of three redox-active components; a central dioxolene,[4,61] the Ni centers, and the terminal phenolates.[8] The one-electron redox process at 75 mV vs Fc^{+}/Fc for **1** is assigned to the central dioxolene unit on the basis of a comparison to the redox properties of a similar Ni salen complex $\mathbf{NiSal^{tBu}}$ ($E_{1/2}$ = 450 mV vs Fc^{+}/Fc).[19] Previous work by Glaser and co-workers also identified the central phloroglucinol unit as the site of oxidation in Ni and Cu triplesalen complexes.[29,30] The present assignment agrees with the DFT calculations on the oxidized complex. The spin density (Figure 5) and predicted bond length changes (Supporting Information, Figure S5) are consistent with oxidation of the central catecholate to form a semiquinone. The spin density is predicted to be distributed to a certain extent over the entire ligand framework, with 18% of the spin density on each of the outer phenolate ligands. It should be noted that DFT calculations tend to overemphasize delocalized, higher symmetry structures.[62] The reversible two-electron redox process for **1** at higher potentials is tentatively assigned to the uncoupled oxidation of the outer phenolate moieties to form phenoxyl radicals. Further experiments were not completed to probe the nature of these highly oxidized species.

Chemical oxidation of **1** in solution with 1 equiv of $AgSbF_6$ ($E_{1/2}$ = 650 mV vs Fc^{+}/Fc in CH_2Cl_2) did not afford the expected cation $[1^{\bullet}]^{+}SbF_6^{-}$ in appreciable yield, even though significant driving force exists for the oxidation.[52] Complexation of the Ag^{+} cation in the binding pocket formed by the four phenolate donors in **1** was confirmed by isolation of the adduct $[1\cdot Ag]^{+}SbF_6^{-}$ in the solid state (Figure 3). This data provided an explanation for the lack of oxidation when using $AgSbF_6$, and is consistent with recent reports of extended Schiff-base systems acting as hosts for metal cations.[27] We therefore used the chemical oxidants NO^{+} SbF_6^{-} and the aminium radical cation $[N(C_6H_3Br_2)_3^{\bullet}]^{+}$ SbF_6^{-} to oxidize **1** in solution. EPR analysis of a frozen solution of $[1^{\bullet}]^{+}$ demonstrates that the unpaired electron is ligand based, with a g_{av} = 2.01 (Figure 4). This value is lower than that for $[\mathbf{NiSal^{tBu\bullet}}]^{+}$ (g_{iso} = 2.045)[17,19] indicating a smaller contribution of the metal to the SOMO of $[1^{\bullet}]^{+}$, and greater ligand radical character. This correlates with the predicted Ni spin density for $[1^{\bullet}]^{+}$ (10%) in comparison to that predicted for $[\mathbf{NiSal^{tBu\bullet}}]^{+}$ (14%).[19] The resonance Raman (rR) spectrum of $[1^{\bullet}]^{+}$ did not exhibit characteristic phenoxyl bands with 413 nm excitation.[53,59] While this could be due to a shift of

dx.doi.org/10.1021/ic200785g |*Inorg. Chem.* 2011, 50, 6746–6755

the phenoxyl bands to higher energy (413 nm is not sufficient for rR excitation[63]), a new intense band is apparent at 1315 cm^{-1} (Figure 8). The band at 1315 cm^{-1} is intermediate between that expected for a catecholate and a semiquinone,[60] and thus we further probed the origin of this transition by DFT. DFT frequency analysis of $[\mathbf{1}^{\bullet}]^{+}$ predicts a vibration at 1352 cm^{-1}, and this band is not present in the predicted Raman spectrum for **1** (Supporting Information, Figure S6). The predicted vibration is a combination of ring stretching modes of the bridging moiety and C−O bond stretches (Supporting Information, Figure S7), fitting with a bridge-localized electronic description for $[\mathbf{1}^{\bullet}]^{+}$. This result contrasts with the work of Thomas et al. on related tetra(salicylidene) phenylenediamine Schiff bases incorporating a 1,2,4,5-tetraiminobenzene bridging unit.[15,23,64] In this case oxidation of both the bimetallic Ni and Cu complexes is delocalized over the salen fragments, with little participation of the bridging unit.[15,23]

A UV−vis−NIR oxidation titration of **1** with $[N(C_6H_3Br_2)_3^{\bullet}]^{+}$ SbF_6^{-} demonstrated clean conversion to the one-electron oxidized form $[\mathbf{1}^{\bullet}]^{+}$ (Figure 6). The oxidation was accompanied by the development of a number of low energy transitions (<15000 cm^{-1}). The two NIR transitions were further probed by TD-DFT calculations, and the predicted bands closely correspond to the experimental transitions (Figure 6). Analysis of the predicted NIR transitions in terms of the molecular orbitals involved allows assignment of the two NIR bands as LLCT transitions with significant electron density transferred from the terminal phenolate moieties to the central bridging unit (Figure 7). In combination, this data is consistent with a description of the overall electronic structure of $[\mathbf{1}^{\bullet}]^{+}$ as bridge-localized.[58] This is in contrast to the mixed-valence ground state for $[\mathbf{NiSal}^{\mathbf{tBu}\bullet}]^{+}$, and analysis in terms of intervalence charge transfer (IVCT).[19]

5. SUMMARY

We have shown in this work that the bimetallic Ni salen complex **1** can be oxidized at a low potential to form a ligand radical species. Analysis of the experimental data, in combination with DFT calculations, has provided insight into the locus of oxidation in $[\mathbf{1}^{\bullet}]^{+}$. Oxidation occurs primarily at the electron rich dioxolene bridge, forming a semiquinone radical with delocalization predicted through the extended π-system of the ligand. On the basis of these studies, $[\mathbf{1}^{\bullet}]^{+}$ is best described as a radical cation with a bridge-localized ground state, rather than as a mixed valence compound. We are currently probing the effect of ligand modifications on radical delocalization and NIR band intensity.

■ ASSOCIATED CONTENT

Supporting Information. Crystallographic data in CIF format. Further details are given in Figures S1−S7 and in a section on the computational data. Full bibliography for ref 42. This material is available free of charge via the Internet at http://pubs.acs.org.

■ AUTHOR INFORMATION

Corresponding Author
*E-mail: tim_storr@sfu.ca.

■ ACKNOWLEDGMENT

This work is supported by a NSERC Discovery Grant (T.S.), and a Grant-in-Aid for Scientific Research (No. 22550055 to Y.S.) from the Ministry of Education, Culture, Sports, Science, and Technology of Japan. Compute Canada and Westgrid are thanked for access to computational resources. Brian O. Patrick is thanked for X-ray analysis. Prof. Charles Walsby and Mike Webb are thanked for assistance with the EPR measurement.

■ REFERENCES

(1) (a) Chirik, P. J.; Wieghardt, K. *Science* **2010**, *327*, 794. (b) Holland, P. L. *Acc. Chem. Res.* **2008**, *41*, 905. (c) De Bruin, B.; Hetterscheid, D. G. H.; Koekkoek, A. J. J.; Grutzmacher, H. *Prog. Inorg. Chem.* **2007**, *55*, 247. (d) Jazdzewski, B. A.; Tolman, W. B. *Coord. Chem. Rev.* **2000**, *200*, 633.

(2) (a) Rogers, M. S.; Dooley, D. M. *Curr. Opin. Chem. Biol.* **2003**, *7*, 189. (b) Stubbe, J.; van der Donk, W. A. *Chem. Rev.* **1998**, *98*, 705.

(3) (a) Thomas, F. *Eur. J. Inorg. Chem.* **2007**, 2379. (b) Whittaker, J. W. *Chem. Rev.* **2003**, *103*, 2347.

(4) (a) Hendrickson, D. N.; Pierpont, C. G. *Top. Curr. Chem.* **2004**, *234*, 63. (b) Pierpont, C. G. *Coord. Chem. Rev.* **2001**, *219*, 415.

(5) (a) Kaim, W.; Schwederski, B. *Pure Appl. Chem.* **2004**, *76*, 351. (b) Ray, K.; Petrenko, T.; Wieghardt, K.; Neese, F. *Dalton Trans* **2007**, 1552.

(6) Pierpont, C. G. *Coord. Chem. Rev.* **2001**, *216*, 99.

(7) (a) Ray, K.; George, S. D.; Solomon, E. I.; Wieghardt, K.; Neese, F. *Chem.—Eur. J.* **2007**, *13*, 2783. (b) Ray, K.; Weyhermuller, T.; Neese, F.; Wieghardt, K. *Inorg. Chem.* **2005**, *44*, 5345.

(8) Chaudhuri, P.; Wieghardt, K. *Prog. Inorg. Chem.* **2001**, *50*, 151.

(9) Thomas, F. In *Stable Radicals: Fundamentals and Applied Aspects of Odd-Electron Compounds*; Hicks, R. G., Ed.; John Wiley and Sons: Chichester, 2010; p 281.

(10) (a) Bachler, V.; Olbrich, G.; Neese, F.; Wieghardt, K. *Inorg. Chem.* **2002**, *41*, 4179. (b) Herebian, D.; Bothe, E.; Neese, F.; Weyhermueller, T.; Weighardt, K. *J. Am. Chem. Soc.* **2003**, *125*, 9116. (c) Mederos, A.; Dominguez, S.; Hernandez-Molina, R.; Sanchiz, J.; Brito, F. *Coord. Chem. Rev.* **1999**, *195*, 913. (d) Peng, S. M.; Chen, C. T.; Liaw, D. S.; Chen, C. I.; Yu, W. *Inorg. Chim. Acta* **1985**, *101*, L31.

(11) (a) Bill, E.; Bothe, E.; Chaudhuri, P.; Chlopek, K.; Herebian, D.; Kokatam, S.; Ray, K.; Weyhermuller, T.; Neese, F.; Wieghardt, K. *Chem.—Eur. J.* **2005**, *11*, 204. (b) Blackmore, K. J.; Sly, M. B.; Haneline, M. R.; Ziller, J. W.; Heyduk, A. F. *Inorg. Chem.* **2008**, *47*, 10522.

(12) Smith, A. L.; Hardcastle, K. I.; Soper, J. D. *J. Am. Chem. Soc.* **2010**, *132*, 14358.

(13) Benisvy, L.; Kannappan, R.; Song, Y. F.; Milikisyants, S.; Huber, M.; Mutikainen, I.; Turpeinen, U.; Garnez, P.; Bernasconi, L.; Baerends, E. J.; Hartl, F.; Reedijk, J. *Eur. J. Inorg. Chem.* **2007**, 631.

(14) (a) Rotthaus, O.; Jarjayes, O.; Del Valle, C. P.; Philouze, C.; Thomas, F. *Chem. Commun.* **2007**, 4462. (b) Rotthaus, O.; Jarjayes, O.; Thomas, F.; Philouze, C.; Del Valle, C. P.; Saint-Aman, E.; Pierre, J. L. *Chem.—Eur. J.* **2006**, *12*, 2293. (c) Shimazaki, Y.; Stack, T. D. P.; Storr, T. *Inorg. Chem.* **2009**, *48*, 8383. (d) Shimazaki, Y.; Yajima, T.; Tani, F.; Karasawa, S.; Fukui, K.; Naruta, Y.; Yamauchi, O. *J. Am. Chem. Soc.* **2007**, *129*, 2559. (e) Orio, M.; Jarjayes, O.; Kanso, H.; Philouze, C.; Neese, F.; Thomas, F. *Angew. Chem., Int. Ed.* **2010**, *49*, 4989. (f) Orio, M.; Philouze, C.; Jarjayes, O.; Neese, F.; Thomas, F. *Inorg. Chem.* **2010**, *49*, 646. (g) Kochem, A.; Orio, M.; Jarjayes, O.; Neese, F.; Thomas, F. *Chem. Commun.* **2010**, *46*, 6765.

(15) Rotthaus, O.; Jarjayes, O.; Philouze, C.; Del Valle, C. P.; Thomas, F. *Dalton Trans.* **2009**, 1792.

(16) (a) Rotthaus, O.; Thomas, F.; Jarjayes, O.; Philouze, C.; Saint-Aman, E.; Pierre, J. L. *Chem.—Eur. J.* **2006**, *12*, 6953. (b) Storr, T.; Verma, P.; Shimazaki, Y.; Wasinger, E. C.; Stack, T. D. P. *Chem.—Eur. J.* **2010**, *16*, 8980.

(17) Shimazaki, Y.; Tani, F.; Fukui, K.; Naruta, Y.; Yamauchi, O. *J. Am. Chem. Soc.* **2003**, *125*, 10512.

(18) Storr, T.; Verma, P.; Pratt, R. C.; Wasinger, E. C.; Shimazaki, Y.; Stack, T. D. P. *J. Am. Chem. Soc.* **2008**, *130*, 15448.

(19) Storr, T.; Wasinger, E. C.; Pratt, R. C.; Stack, T. D. P. *Angew. Chem., Int. Ed.* **2007**, *46*, 5198.

(20) (a) Adhikari, D.; Mossin, S.; Basuli, F.; Huffman, J. C.; Szilagyi, R. K.; Meyer, K.; Mindiola, D. J. *J. Am. Chem. Soc.* **2008**, *130*, 3676. (b) Blackmore, K. J.; Lal, N.; Ziller, J. W.; Heyduk, A. F. *J. Am. Chem. Soc.* **2008**, *130*, 2728. (c) Buttner, T.; Geier, J.; Frison, G.; Harmer, J.; Calle, C.; Schweiger, A.; Schonberg, H.; Grutzmacher, H. *Science* **2005**, *307*, 235. (d) Haneline, M. R.; Heyduk, A. F. *J. Am. Chem. Soc.* **2006**, *128*, 8410. (e) Konigsmann, M.; Donati, N.; Stein, D.; Schonberg, H.; Harmer, J.; Sreekanth, A.; Grutzmacher, H. *Angew. Chem., Int. Ed.* **2007**, *46*, 3567. (f) Maire, P.; Konigsmann, M.; Sreekanth, A.; Harmer, J.; Schweiger, A.; Grutzmacher, H. *J. Am. Chem. Soc.* **2006**, *128*, 6578. (g) Miyazato, Y.; Wada, T.; Tanaka, K. *Bull. Chem. Soc. Jpn.* **2006**, *79*, 745. (h) Ringenberg, M. R.; Kokatam, S. L.; Heiden, Z. M.; Rauchfuss, T. B. *J. Am. Chem. Soc.* **2008**, *130*, 788. (i) Bart, S. C.; Chlopek, K.; Bill, E.; Bouwkamp, M. W.; Lobkovsky, E.; Neese, F.; Wieghardt, K.; Chirik, P. J. *J. Am. Chem. Soc.* **2006**, *128*, 13901. (j) Zarkesh, R. A.; Ziller, J. W.; Heyduk, A. F. *Angew. Chem., Int. Ed.* **2008**, *47*, 4715. (k) Atienza, C. C. H.; Bowman, A. C.; Lobkovsky, E.; Chirik, P. J. *J. Am. Chem. Soc.* **2010**, *132*, 16343. (l) Tondreau, A. M.; Milsmann, C.; Patrick, A. D.; Hoyt, H. M.; Lobkovsky, E.; Wieghardt, K.; Chirik, P. J. *J. Am. Chem. Soc.* **2010**, *132*, 15046.

(21) (a) Baleizao, C.; Garcia, H. *Chem. Rev.* **2006**, *106*, 3987. (b) Canali, L.; Sherrington, D. C. *Chem. Soc. Rev.* **1999**, *28*, 85. (c) Darensbourg, D. J. *Chem. Rev.* **2007**, *107*, 2388. (d) Jacobsen, E. N. *Acc. Chem. Res.* **2000**, *33*, 421. (e) McGarrigle, E. M.; Gilheany, D. G. *Chem. Rev.* **2005**, *105*, 1563.

(22) (a) Abuelwafa, S. M.; Issa, R. M.; McAuliffe, C. A. *Inorg. Chim. Acta* **1985**, *99*, 103. (b) Audebert, P.; Capdevielle, P.; Maumy, M. *New J. Chem.* **1991**, *15*, 235. (c) Bottcher, A.; Elias, H.; Jager, E. G.; Langfelderova, H.; Mazur, M.; Muller, L.; Paulus, H.; Pelikan, P.; Rudolph, M.; Valko, M. *Inorg. Chem.* **1993**, *32*, 4131. (d) Freire, C.; de Castro, B. *J. Chem. Soc., Dalton Trans.* **1998**, 1491. (e) Pasini, A.; Bernini, E.; Scaglia, M.; DeSantis, G. *Polyhedron* **1996**, *15*, 4461.

(23) Rotthaus, O.; Jarjayes, O.; Thomas, F.; Philouze, C.; Saint-Aman, E.; Pierre, J. L. *Dalton Trans.* **2007**, 889.

(24) Freire, C.; de Castro, B. *Polyhedron* **1998**, *17*, 4227.

(25) (a) Belokon, Y. N.; Green, B.; Ikonnikov, N. S.; North, M.; Tararov, V. I. *Tetrahedron Lett.* **1999**, *40*, 8147. (b) Larrow, J. F.; Schaus, S. E.; Jacobsen, E. N. *J. Am. Chem. Soc.* **1996**, *118*, 7420. (c) Mazet, C.; Jacobsen, E. N. *Angew. Chem., Int. Ed.* **2008**, *47*, 1762. (d) Haak, R. M.; Belmonte, M. M.; Escudero-Adan, E. C.; Benet-Buchholz, J.; Kleij, A. W. *Dalton Trans.* **2010**, *39*, 593. (e) Wezenberg, S. J.; Kleij, A. W. *Adv. Synth. Catal.* **2010**, *352*, 85. (f) Konsler, R. G.; Karl, J.; Jacobsen, E. N. *J. Am. Chem. Soc.* **1998**, *120*, 10780. (g) Mukherjee, C.; Stammler, A.; Bogge, H.; Glaser, T. *Chem.—Eur. J.* **2010**, *16*, 10137. (h) Shibasaki, M.; Kanai, M.; Matsunaga, S.; Kumagai, N. *Acc. Chem. Res.* **2009**, *42*, 1117. (i) Thomas, R. M.; Widger, P. C. B.; Ahmed, S. M.; Jeske, R. C.; Hirahata, W.; Lobkovsky, E. B.; Coates, G. W. *J. Am. Chem. Soc.* **2010**, *132*, 16520. (j) Huang, Y.; Liu, T.; Lin, J.; Luì, J.; Lin, Z.; Cao, R. *Inorg. Chem.* **2011**, *50*, 2191.

(26) (a) Wezenberg, S. J.; Salassa, G.; Escudero-Adan, E. C.; Benet-Buchholz, J.; Kleij, A. W. *Angew. Chem., Int. Ed.* **2011**, *50*, 713. (b) Jiang, J.; MacLachlan, M. J. *Chem. Commun.* **2009**, 5695. (c) Guo, Z. Q.; Tong, W. L.; Chan, M. C. W. *Chem. Commun.* **2009**, 6189.

(27) (a) Akine, S.; Taniguchi, T.; Nabeshima, T. *J. Am. Chem. Soc.* **2006**, *128*, 15765. (b) Akine, S.; Utsuno, F.; Nabeshima, T. *Chem. Commun.* **2010**, *46*, 1029.

(28) (a) Glaser, T.; Heidemeier, M.; Frohlich, R. *C. R. Chim.* **2007**, *10*, 71. (b) von Richthofen, C. G. F.; Stammler, A.; Bogge, H.; Glaser, T. *Eur. J. Inorg. Chem.* **2011**, 49. (c) Feltham, H. L. C.; Clerac, R.; Brooker, S. *Dalton Trans.* **2009**, 2965.

(29) Glaser, T.; Heidemeier, M.; Strautmann, J. B. H.; Bogge, H.; Stammler, A.; Krickemeyer, E.; Huenerbein, R.; Grimme, S.; Bothe, E.; Bill, E. *Chem.—Eur. J.* **2007**, *13*, 9191.

(30) Glaser, T.; Heidemeler, M.; Frohlich, R.; Hildebrandt, P.; Bothe, E.; Bill, E. *Inorg. Chem.* **2005**, *44*, 5467.

(31) (a) Frischmann, P. D.; Guieu, S.; Tabeshi, R.; MacLachlan, M. J. *J. Am. Chem. Soc.* **2010**, *132*, 7668. (b) Wu, H. C.; Thanasekaran, P.; Tsai, C. H.; Wu, J. Y.; Huang, S. M.; Wen, Y. S.; Lu, K. L. *Inorg. Chem.* **2006**, *45*, 295. (c) Yoshida, N.; Oshio, H.; Ito, T. *Chem. Commun.* **1998**, 63.

(32) (a) Hui, J. K. H.; Frischmann, P. D.; Tso, C. H.; Michal, C. A.; MacLachlan, M. J. *Chem.—Eur. J.* **2010**, *16*, 2453. (b) Ma, C. T. L.; MacLachlan, M. J. *Angew. Chem., Int. Ed.* **2005**, *44*, 4178.

(33) (a) Akine, S.; Taniguchi, T.; Nabeshima, T. *Tetrahedron Lett.* **2001**, *42*, 8861. (b) Gallant, A. J.; MacLachlan, M. J. *Angew. Chem., Int. Ed.* **2003**, *42*, 5307.

(34) Frischmann, P. D.; Facey, G. A.; Ghi, P. Y.; Gallant, A. J.; Bryce, D. L.; Lelj, F.; MacLachlan, M. J. *J. Am. Chem. Soc.* **2010**, *132*, 3893.

(35) Perrin, D. D.; Armarego, W. L. F. *Purification of Laboratory Chemicals*, 1st ed.; Pergamon Press: New York, 1988.

(36) Michellys, P. Y. *J. Med. Chem.* **2003**, *46*, 2683.

(37) Bjorn, A. . Ph.D. Thesis, University of Cincinnati, Cincinnati, Ohio, 2002.

(38) Stoll, S.; Schweiger, A. *J. Magn. Reson.* **2006**, *178*, 42.

(39) *SIR97*; Altomare, A.; Burla, M. C.; Camalli, M.; Cascarano, G. L.; Giacovazzo, C.; Guagliardi, A.; Moliterni, A. G. G.; Polidori, G.; Spagna, R. *J. Appl. Crystallogr.* **1999**, *32*, 115.

(40) van der Sluis, P.; Spek, A. L. *Acta Crystallogr., Sect. A* **1990**, *46*, 194.

(41) Betteridge, P. W.; Carruthers, J. R.; Cooper, R. I.; Prout, K.; Watkin, D. J. *J. Appl. Crystallogr.* **2003**, *36*, 1487.

(42) Frisch, M. J. T., et al. *Gaussian 09*, Revision A.02; Gaussian, Inc.: Wallingford, CT, 2009.

(43) (a) Becke, A. D. *J. Chem. Phys.* **1993**, *98*, 5648. (b) Stephens, P. J.; Devlin, F. J.; Chabalowski, C. F.; Frisch, M. J. *J. Phys. Chem.* **1994**, *98*, 11623.

(44) (a) Schafer, A.; Horn, H.; Ahlrichs, R. *J. Chem. Phys.* **1992**, *97*, 2571. (b) Schafer, A.; Huber, C.; Ahlrichs, R. *J. Chem. Phys.* **1994**, *100*, 5829.

(45) Casida, M. E. In In *Recent Advances in Density Functional Methods*; Chong, D. P., Ed.; World Scientific: Singapore, 1995; p 155.

(46) Stratmann, R. E.; Scuseria, G. E.; Frisch, M. J. *J. Chem. Phys.* **1998**, *109*, 8218.

(47) (a) Barone, V.; Cossi, M.; Tomasi, J. *J. Chem. Phys.* **1997**, *107*, 3210. (b) Barone, V.; Cossi, M.; Tomasi, J. *J. Comput. Chem.* **1998**, *19*, 404. (c) Miertus, S.; Scrocco, E.; Tomasi, J. *Chem. Phys.* **1981**, *55*, 117. (d) Tomasi, J.; Mennucci, B.; Cances, E. *J. Mol. Struct.* **1999**, *464*, 211.

(48) (a) Gorelsky, S. I. *AOMix: Program for Molecular Orbital Analysis*, http://www.sg-chem.net/ 2007, University of Ottawa, Canada; (b) Gorelsky, S. I.; Lever, A. B. P. *J. Organomet. Chem.* **2001**, *635*, 187. (c) Gorelsky, S. I.; Solomon, E. I. *Theor. Chem. Acc.* **2008**, *119*, 57.

(49) Bottcher, A.; Elias, H.; Eisenmann, B.; Hilms, E.; Huber, A.; Kniep, R.; Rohr, C.; Zehnder, M.; Neuburger, M.; Springborg, J. *Z. Naturforsch. B* **1994**, *49*, 1089.

(50) Thomas, F.; Jarjayes, O.; Duboc, C.; Philouze, C.; Saint-Aman, E.; Pierre, J.-L. *Dalton Trans.* **2004**, 2662.

(51) The first ligand-based redox couple for a monometallica Ni salen depends on the nature of the diamine backbone and the electron withdrawing or donating effect of the substituents on the pheonlates. In this work **NiSal^{tBu}** was chosen as monomeric analogue to **1**.

(52) Connelly, N. G.; Geiger, W. E. *Chem. Rev.* **1996**, *96*, 877.

(53) Sokolowski, A.; Muller, J.; Weyhermuller, T.; Schnepf, R.; Hildebrandt, P.; Hildenbrand, K.; Bothe, E.; Wieghardt, K. *J. Am. Chem. Soc.* **1997**, *119*, 8889.

(54) (a) Drago, R. S.; Baucom, E. I. *Inorg. Chem.* **1972**, *11*, 2064. (b) Kruger, H. J.; Holm, R. H. *Inorg. Chem.* **1987**, *26*, 3645. (c) Ottenwaelder, X.; Ruiz-Garcia, R.; Blondin, G.; Carasco, R.; Cano, J.; Lexa, D.; Journaux, Y.; Aukauloo, A. *Chem. Commun.* **2004**, 504.

(55) Shimazaki, Y.; Arai, N.; Dunn, T. J.; Yajima, T.; Tani, F.; Ramogida, C. F.; Storr, T. *Dalton Trans.* **2011**, *40*, 2469.

(56) (a) Creutz, C.; Taube, H. *J. Am. Chem. Soc.* **1969**, *91*, 3988. (b) Hush, N. S. *Prog. Inorg. Chem.* **1967**, *8*, 391. (c) Robin, M. B.; Day, P. *Adv. Inorg. Chem. Radiochem.* **1967**, *10*, 247.

(57) Stratmann, R. E.; Scuseria, G. E.; Frisch, M. J. *J. Chem. Phys.* **1998**, *109*, 8218.

(58) (a) Lambert, C.; Amthor, S.; Schelter, J. *J. Phys. Chem. A* **2004**, *108*, 6474. (b) Armitt, D. J.; Bruce, M. I.; Gaudio, M.; Zaitseva, N. N.; Skelton, B. W.; White, A. H.; Le Guennic, B.; Halet, J. F.; Fox, M. A.; Roberts, R. L.; Hartl, F.; Low, P. J. *Dalton Trans* **2008**, 6763. (c) Kaim, W.; Lahiri, G. K. *Angew. Chem., Int. Ed.* **2007**, *46*, 1778. (d) Man, W. Y.; Xia, J.-L.; Brown, N. J.; Farmer, J. D.; Yufit, D. S.; Howard, J. A. K.; Liu, S. H.; Low, P. J. *Organometallics* **2011**, *30*, 1852–1858.

(59) (a) Mukherjee, A.; McGlashen, M. L.; Spiro, T. G. *J. Phys. Chem.* **1995**, *99*, 4912. (b) Sokolowski, A.; Leutbecher, H.; Weyhermuller, T.; Schnepf, R.; Both, E.; Bill, E.; Hildebrandt, P.; Wieghardt, K. *J. Biol. Inorg. Chem.* **1997**, *2*, 444.

(60) Vlcek, A. *Comments Inorg. Chem.* **1994**, *16*, 207.

(61) Pierpont, C. G.; Lange, C. W. *Prog. Inorg. Chem.* **1994**, *41*, 331.

(62) Cramer, C. J. *Essentials of Computational Chemistry*, 2nd ed.; Wiley: West Sussex, England, 2004.

(63) Kurahashi, T.; Kikuchi, A.; Tosha, T.; Shiro, Y.; Kitagawa, T.; Fuji, H. *Inorg. Chem.* **2008**, *47*, 1674.

(64) Chichak, K.; Jacquemard, U.; Branda, N. R. *Eur. J. Inorg. Chem.* **2002**, 357.